# "Focusing" eikonal equation and global tomography

*Biondo Biondi, Sergey Fomel, and Tariq Alkhalifah*[1]

**ABSTRACT**

The transformation of the eikonal equation from depth coordinates $(z,x)$ into vertical-traveltime coordinates $(\tau,\xi)$ enables the computation of reflections traveltimes independent of depth-mapping. This separation allows the focusing and mapping steps to be performed sequentially even in the presence of complex velocity functions, that otherwise would "require" depth migration.

The traveltimes satisfying the transformed eikonal equation can be numerically evaluated by solving the associated ray tracing equations. The application of Fermat's principle leads to the expression of linear relationships between perturbations in traveltimes and perturbations in focusing velocity. This linearization, in conjunction with ray tracing, can be used for a tomographic estimation of focusing velocity.

## INTRODUCTION

Velocity has a dual role in reflection-seismic imaging. It is needed to focus the data through migration, and to map the reflectors in depth by converting arrival times into depths. These two imaging goals are often conflicting. The velocity function that best focuses the data is not necessarily the velocity that performs the correct depth mapping.

The *focusing* velocity is the velocity that best predicts the relative delays between reflections originated at the same point in the subsurface and recorded at different offsets and midpoints. We can measure these relative delays and try to estimate the focusing velocity by solving an inverse problem. On the contrary, the *mapping* velocity mostly affects the absolute delays of the reflections. If we do not know the depth of the reflectors, we cannot estimate the mapping velocity from reflection data. To estimate mapping velocity we need other source of information, such as well data and a priori geological information.

This distinction between focusing and mapping velocity is routinely used when the data it time imaged, and is one of the source of robustness of the time-imaging procedure. In time imaging, the data are first focused by determining stacking and/or RMS velocities, then map-migrated to depth along the image rays using an appropriate mapping velocity (Hubral, 1977; Larner et al., 1981). Unfortunately this useful separation is lost when the data are imaged using depth migration. In this case the same velocity field is used to focus the data and to map

[1]**email:** biondo@sep.stanford.edu,sergey@sep.stanford.edu,tariq@sep.stanford.edu

the reflectors. The main reason for this shortcoming of depth migration is not conceptual, but it is imposed by limitations in current depth-migration algorithms. In this paper we present a method for computing migration operators for Kirchhoff-like migrations as a function of the focusing velocity. The method is based on a coordinate transformation from depth to two-way vertical traveltime applied to the eikonal equation. We demonstrate that under fairly mild assumptions on the relation between focusing and mapping velocities, the traveltimes computed using the transformed eikonal are only functions of the focusing velocity. As a result, we call the transformed eikonal equation the *focusing eikonal*.

The focusing eikonal has potential applications to the estimation of focusing velocities. It enables us to apply to depth-migration problems the same sequential estimation of the two interval velocities that is possible in time imaging. One problem with the joint estimation of the two velocities is that a velocity perturbation not only causes changes in the focusing of the data but it also causes a vertical shift of both the reflectors and velocity that are below the perturbation. These vertical shifts present a challenge to reflection tomography, and are one of the reasons why layer-stripping procedures are considered to be more robust than global tomographic procedures. However, because global tomography has the potential to be more accurate than layer stripping, there are many incentives to stabilizing global tomography. We propose to perform the whole velocity estimation in the vertical traveltime domain. When the velocity function and the reflector geometry are expressed in the vertical-traveltime coordinates, their position is only weakly dependent on velocity. Therefore, we may ameliorate the problems associated with inaccuracies in the mapping velocity.

## FOCUSING EIKONAL EQUATION

To derive the focusing eikonal equation we apply a coordinates transformation from depth ($z$) to two-ways vertical traveltime ($\tau$) to the eikonal of the acoustic wave equation. The eikonal for the arrival time $t$ of high-frequency acoustic waves is

$$V_m(z,x)^2\left[\frac{\partial t(z,x)}{\partial z}\right]^2 + V_f(z,x)^2\left[\frac{\partial t(z,x)}{\partial x}\right]^2 = 1, \tag{1}$$

where $V_m$ and $V_f$ are respectively the **mapping velocity** and the **focusing velocity**. Because we are interested to analyze the effects of focusing and mapping velocities on reflection traveltimes, we kept the $V_f$ and $V_m$ distinguished in equation (1). Although this equation is valid for a general elliptical anisotropic medium, in this paper we focus on isotropic media. A companion paper discusses the focusing eikonal for a general transversely isotropic media with a vertical axis of symmetry. (Alkhalifah et al., 1997).

The mapping between the depth $(z,x)$ and the vertical traveltime $(\tau,\xi)$ domain are defined by the following transformation of coordinates:

$$\tau(z,x) = \int_0^z \frac{2}{V\left(z',x\right)}dz' \tag{2}$$

$$\xi(z,x) = x. \tag{3}$$

This transformation implies the following relationships between the partial derivatives of the traveltime that appear in the eikonal equation (1):

$$\frac{\partial t}{\partial z} = \frac{\partial t}{\partial \tau}\frac{\partial \tau}{\partial z}+\frac{\partial t}{\partial \xi}\frac{\partial \xi}{\partial z}=\frac{\partial t}{\partial \tau}\frac{2}{V_m(z,x)} \tag{4}$$

$$\frac{\partial t}{\partial x} = \frac{\partial t}{\partial \xi}\frac{\partial \xi}{\partial x}+\frac{\partial t}{\partial \tau}\frac{\partial \tau}{\partial x}=\frac{\partial t}{\partial \xi}+\frac{\partial t}{\partial \tau}\int_0^z \frac{\partial}{\partial x}\left[\frac{2}{V_m\left(z^{'},x\right)}\right]dz^{'}=\frac{\partial t}{\partial \xi}+\frac{\partial t}{\partial \tau}\sigma_m. \tag{5}$$

Substituting these partial derivatives in the eikonal equation (1) we derive the **focusing eikonal** equation

$$4\left[\frac{\partial t(\tau,\xi)}{\partial \tau}\right]^2+V_f(\tau,\xi)^2\left[\frac{\partial t(\tau,\xi)}{\partial \xi}+\sigma_m(\tau,\xi)\frac{\partial t(\tau,\xi)}{\partial \tau}\right]^2=1. \tag{6}$$

The focusing eikonal depends directly from the the focusing velocity but only indirectly from the mapping velocity, through the **differential mapping factor** $\sigma_m$. Furthermore, because $\sigma_m$ is the vertical integral of the horizontal derivative of $V_m$, when $V_m$ is assumed to be proportional to $V_f$ with a constant of proportionality that is only function of depth; that is,

$$V_m(z,x)=\alpha(z)\,V_f(z,x), \tag{7}$$

the focusing eikonal becomes independent from $V_m$.

This property is easily demonstrated by performing the change of variable from $z$ to $\tau$ defined in equation (2) in the integral that defines $\sigma_m$ in equation (5). After this change of variable the expression for $\sigma_m$ as a function of $\tau$ becomes

$$\sigma_m(\tau,x) = \int_0^\tau V_m\left(\tau^{'},x\right)\frac{\partial}{\partial x}\left[\frac{1}{V_m\left(\tau^{'},x\right)}\right]d\tau^{'}=$$

$$\sigma_f(\tau,x) = \int_0^\tau V_f\left(\tau^{'},x\right)\frac{\partial}{\partial x}\left[\frac{1}{V_f\left(\tau^{'},x\right)}\right]d\tau^{'}. \tag{8}$$

In the companion paper (1997) we analyze the errors caused by assuming $\sigma_m$ equal to $\sigma_f$ when the condition of equation (7) in not exactly fulfilled.

The previous result demonstrates that, as long as the condition of equation (7) is satisfied, reflection data can be focused without knowledge of the mapping velocity, and thus that the focusing step and the mapping step can be performed sequentially.

Notice that in an horizontally stratified medium the focusing eikonal becomes the eikonal for an elliptical anisotropic medium with normalized vertical "velocity" equal to 2. If the velocity is laterally varying, neglecting $\sigma_f$ is equivalent to neglecting the thin-lens term in finite-difference time migration (Hatton et al., 1981). Raynaud and Thore (1993) used this approximation to trace rays in the $\tau$ domain.

The presence of the differential mapping factor $\sigma_f$ in the focusing eikonal makes the separation of the mapping and the focusing processes imperfect. Therefore the eikonal in

equation (1) should be properly called *quasi-focusing*. An interesting development would be to substitute for the transformation of variables defined by equations (2) and (3) a different transformation of variables for which $\sigma_f$ would be uniformly zero even in a laterally varying medium. We speculate that this transformation of variable is the one induced by the image rays (Hubral, 1977).

Finally we should notice that the expressions for evaluating $\sigma_f$ given in equation (5), or even in equation (8), are not convenient when working in the $(\tau,\xi)$ domain, because they require the evaluation of spatial derivatives in the $(z,x)$. It can be easily demonstrated that $\sigma_f$ can be evaluated using the following expression,

$$\sigma_f(\tau,\xi) = -\frac{2}{V_f(\tau,\xi)}\frac{\partial z}{\partial \xi} = -\frac{1}{V_f(\tau,\xi)}\int_0^\tau \frac{\partial V_f\left(\tau',\xi\right)}{\partial \xi} d\tau'. \tag{9}$$

**Ray tracing in** $(\tau,\xi)$

The solutions to the focusing eikonal can be computed using current methods for solving the standard eikonal, either directly by modern eikonal solvers (Sethian and Popovici, 1997; Fomel, 1997), or by ray tracing. We chose a ray tracing solution, because for reflection tomography is handier to have rays than traveltime maps.

To derive the ray-tracing system for the focusing eikonal we begin by writing its associated Hamiltonian as a function of the ray parameters $p_\tau$ and $p_\xi$,

$$H\left(\tau,\xi,p_\tau,p_\xi\right) = \frac{1}{2}\left\{4p_\tau^2 + V_f^2\left[p_\xi + \sigma_f p_\tau\right]^2\right\}. \tag{10}$$

The associated ray-tracing equation are:

$$\begin{aligned}
\frac{d\xi}{dt} &= \frac{\partial H}{\partial p_\xi} = V_f^2\left(p_\xi + \sigma_f p_\tau\right) \\
\frac{d\tau}{dt} &= \frac{\partial H}{\partial p_\tau} = V_f^2\sigma_f\left(p_\xi + \sigma_f p_\tau\right) + 4p_\tau \\
\frac{dp_\xi}{dt} &= -\frac{\partial H}{\partial \xi} = -\left[\left(p_\xi + \sigma_f p_\tau\right)^2 V_f\frac{\partial V_f}{\partial \xi} + V_f^2 p_\tau\left(p_\xi + \sigma_f p_\tau\right)\frac{\partial \sigma_f}{\partial \xi}\right] \\
\frac{dp_\tau}{dt} &= -\frac{\partial H}{\partial \tau} = -\left[\left(p_\xi + \sigma_f p_\tau\right)^2 V_f\frac{\partial V_f}{\partial \tau} + V_f^2 p_\tau\left(p_\xi + \sigma_f p_\tau\right)\frac{\partial \sigma_f}{\partial \tau}\right].
\end{aligned} \tag{11}$$

Rays can be traced in $(\tau,\xi)$ by solving the ray-tracing equations in (11) by a standard ODE solver. The appropriate initial conditions for the ray parameters $p_\tau$ and $p_\xi$ when the source is at $(\tau_0,\xi_0)$ and the take-off angle is $\theta_\tau$ are:

$$\begin{aligned}
p_{\tau_0} &= \frac{\cos\theta_\tau}{2} \\
p_{\xi_0} &= \left[\frac{\sin\theta_\tau}{V(\tau_0,\xi_0)} - \sigma_f(\tau_0,\xi_0)\, p_{\tau_0}\right].
\end{aligned} \tag{12}$$

To test the accuracy of our derivations we numerically solved the ray tracing equations (11) for a heterogeneous velocity function, and compared the results with a ray-tracing solution of the standard eikonal equation. As expected, $\tau$-rays map exactly into $z$-rays, for all velocity fields. Figure 1 and Figure 2 show an example of the ray field when the velocity function is a Gaussian-shaped negative velocity anomaly superimposed onto a constant velocity background. Notice that the focusing eikonal handles correctly the caustic and wavefront triplication below the anomaly. Figure 3 shows the effects of neglecting the differential mapping factor $\sigma_f$. It shows the $\tau$-rays computed setting $\sigma_f$ to zero, and remapped into $(z,x)$. The wavefronts are distorted compared to the true wavefronts shown in Figure 1

## REFLECTION TOMOGRAPHY IN $(\tau,\xi)$

One of the potential application of the focusing eikonal is reflection tomography. Because both the velocity function and the reflectors are more "stationary" in the $(\tau,\xi)$ domain than in the $(z,x)$, we speculate that reflection tomography performed in $(\tau,\xi)$ is more stable than reflection tomography performed in $(z,x)$.

To perform reflection tomography, in addition to ray tracing, we need to compute the gradient of traveltimes with respect to the velocity function and to handle correctly the reflections at the boundaries. Appendix A shows the relationships between the ray parameters of the incident and reflected $\tau$-rays at a planar interface. In this section we derive the traveltime gradients for $\tau$-rays. The derivation is straightforward and is based on Fermat principle applied to the $\tau$-rays.

The transformation of variables defined in equations (2) and (3) implies the following relationships between the differential quantities $(dz,dx)$ and $(d\tau,d\xi)$.

$$dz = \frac{V_m}{2}d\tau - \frac{V_m\sigma_f}{2}d\xi \tag{13}$$

$$dx = d\xi. \tag{14}$$

Applying this transformations to the expression of the time increment along a $z$-ray, leads to the equivalent expression for the the time increment along a $\tau$-ray,

$$dt = \sqrt{\frac{dz^2}{V_m^2}+\frac{dx^2}{V_f^2}} = \sqrt{\left(\frac{d\tau-\sigma_f d\xi}{2}\right)^2 + S_f^2 d\xi^2}, \tag{15}$$

where $S_f$ is the focusing slowness. The first derivative of the time increment $dt$ with respect to the focusing slowness is given by

$$\frac{d(dt)}{dS_f} = \frac{\widetilde{S}_f d\xi^2}{\sqrt{\left(\frac{d\tau-\widetilde{\sigma}_f d\xi}{2}\right)^2 + \widetilde{S}_f{}^2 d\xi^2}}\frac{d\widetilde{S}_f}{dS_f} - \frac{\left(d\tau-\widetilde{\sigma}_f d\xi\right)d\xi}{4\sqrt{\left(\frac{d\tau-\widetilde{\sigma}_f d\xi}{2}\right)^2 + \widetilde{S}_f{}^2 d\xi^2}}\frac{d\widetilde{\sigma}_f}{dS_f} \tag{16}$$

$$= \frac{\widetilde{S}_f d\xi^2}{\widetilde{dt}}\frac{d\widetilde{S}_f}{dS_f} - \frac{\left(d\tau-\widetilde{\sigma}_f d\xi\right)d\xi}{4\widetilde{dt},}\frac{d\widetilde{\sigma}_f}{dS_f} \tag{17}$$

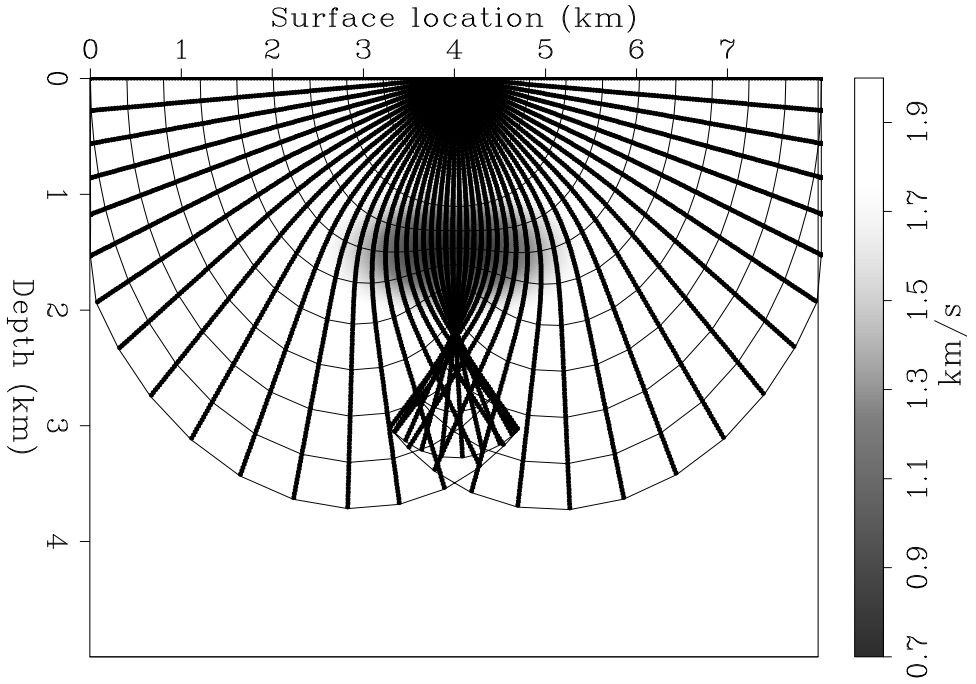


Figure 1: Ray field in $(z,x)$ domain with a negative velocity anomaly in constant background. foceiko-Raytau-z-an [NR]

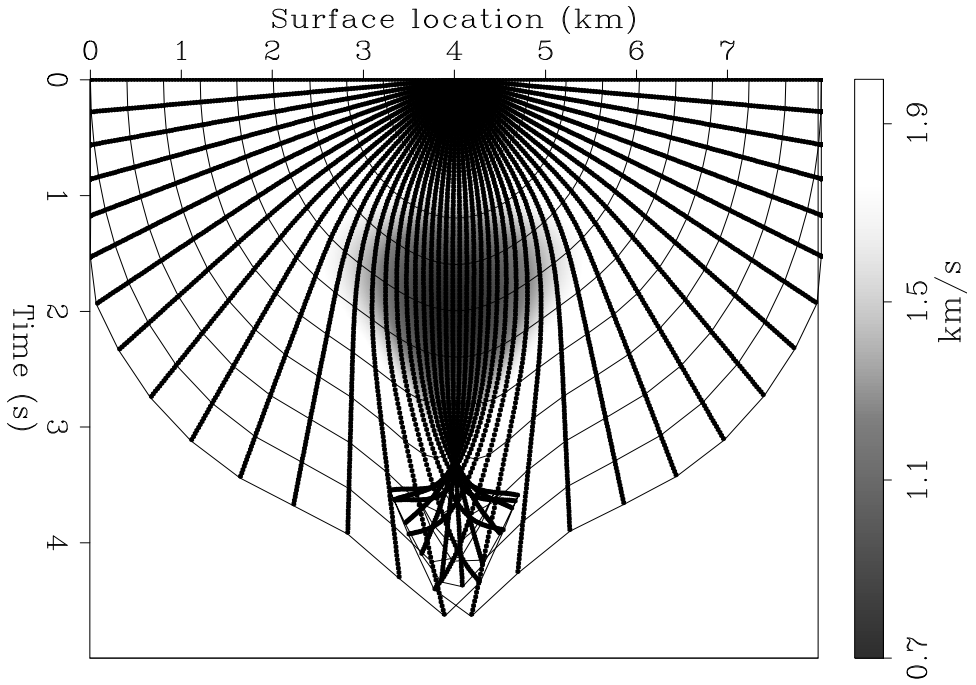


Figure 2: Ray field in $(\tau,\xi)$ domain with a negative velocity anomaly in constant background. This ray field maps exactly into the one shown in Figure 1. foceiko-Raytau-an [NR]

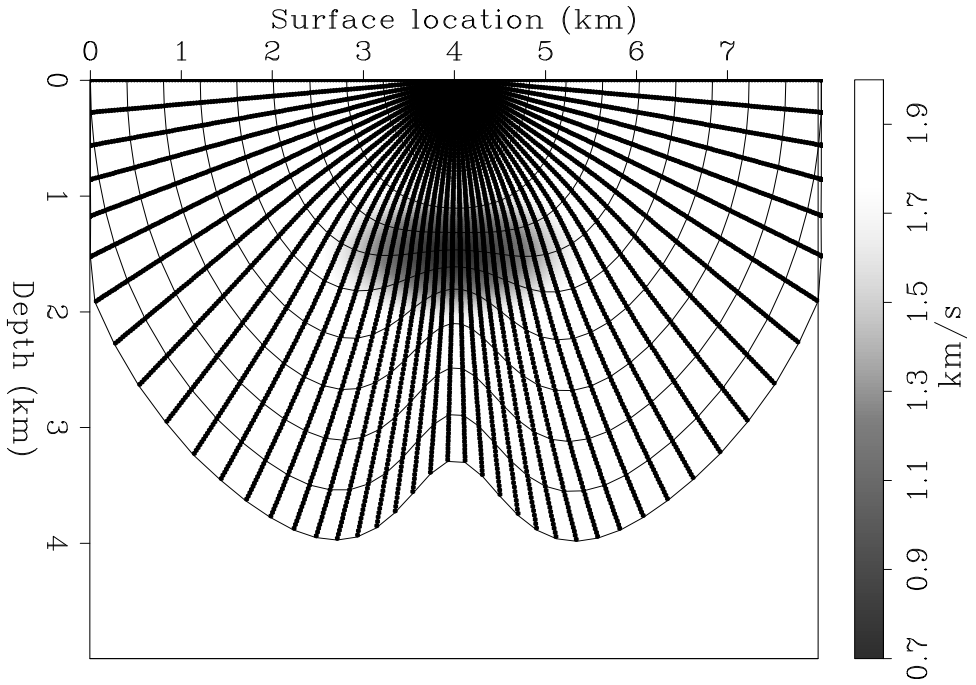


Figure 3: Ray field in $(z,x)$ domain computed assuming the differential mapping factor $\sigma$ equal to zero. This ray field is different than the one shown i n Figure 1. foceiko-Raytau-ell-z-an [NR]

where the tildes on the variables indicate that they are evaluated along the raypath.

Applying Fermat principle, the first order perturbations in the traveltimes $\Delta t$ caused by perturbations in slowness $\Delta S_f$ are given by the following integral evaluated along the unperturbed raypath $\tau$-ray,

$$\Delta t = \int_{\tau-\text{ray}} \frac{d\,(dt)}{dS_f} \Delta S_f \;\; dl, \tag{18}$$

where $dl$ is the path-length increment. Notice that the $\tau$-ray is not stationary in the $(z,x)$ domain, but that the term in equation (17) that includes $\widetilde{\sigma_f}$ takes into account the perturbation of the raypath in the $(z,x)$ domain.

**Tracking reflectors movements**

One of the most challenging problems of reflection tomography is to track correctly the movement of reflectors caused by changes in velocity. Usually the reflectors are parametrized independently from velocity and large reflectors movement can cause instability in the inversion process. One of the potential advantages of $(\tau,\xi)$ tomography over $(z,x)$ tomography is that reflectors move less in the $(\tau,\xi)$ than in the $(z,x)$ domain, and that they move more consistently with the velocity function.

This reflector movement caused by velocity perturbations can be subdivided in a *residual migration* component and a *residual mapping* component. One of the advantages of $(\tau,\xi)$ tomography is that the residual mapping is automatically taken into account by the linearization introduced in equation (17). In contrast, $(z,x)$ tomography has an additional term to take into account both the residual mapping and migration effects. In the examples shown in this paper we used the following adaptation of the expression presented by Stork and Clayton (1991) to correct for the residual mapping in $(z,x)$ tomography:

$$\Delta t = \Delta z \left( p_{z\Downarrow} + p_{z\Uparrow} \right), \tag{19}$$

where $\Delta z$ is the reflector vertical movement, while $p_{z\Downarrow}$ and $p_{z\Uparrow}$ are respectively the vertical ray parameters of the incident and reflected rays at the reflection point. To be consistent in the comparison between $(\tau,\xi)$ domain tomography and $(z,x)$ domain tomography, we computed $\Delta z$ as a residual mapping term along the vertical path. The residual migration term could be computed by performing a residual map migration of the zero-offset arrivals. This residual migration term could be added to both $(\tau,\xi)$ domain tomography and $(z,x)$ domain tomography. For $(\tau,\xi)$ tomography the expression linking the $\Delta\tau$ caused by residual migration to the corresponding traveltime perturbations would be similar to equation (19); that is,

$$\Delta t = \Delta \tau \left( p_{\tau\Downarrow} + p_{\tau\Uparrow} \right). \tag{20}$$

**Comparing linearizations of forward modeling in $(\tau,\xi)$ and $(z,x)$**

One of the motivations for performing tomography in $(\tau,\xi)$ domain is to improve the linearity of the forward modeling problem. Therefore, we compare the accuracy of the linearized forward modeling for the $(\tau,\xi)$ tomography with the linearized forward modeling for the $(z,x)$ tomography in a few significant examples. To make this comparison we define a reflector geometry, and a velocity model, that we call the "true" model. The true model is defined as a velocity anomaly superimposed onto a background model. Then we define a starting velocity model and a starting reflector geometry. We assume that the starting model was estimated by interpreting a migrated section, therefore the starting velocity model in the $(\tau,\xi)$ domain is equal to the background model in the $(\tau,\xi)$ domain. The starting model in the $(z,x)$ domain is defined by the starting model in the $(\tau,\xi)$ domain mapped into depth. Notice that while both the true and the starting models map into each other according to the mapping defined in equations (2) and (3), their perturbations do not. The starting reflector geometry is the results of map-migrating the true zero-offset arrivals assuming the starting velocity model.

To analyze the linearity of the forward modeling, we compare the linearization errors of the two different tomographic methods. We define the linearization errors as the differences between the reflection traveltimes modeled with the true model, and the reflection traveltimes that are predicted by linearizing the forward modeling at the starting model. To compute the traveltimes perturbations we set as velocity perturbations the difference between the true model and the starting model.

The true model for the first example is a positive Gaussian-shaped velocity anomaly with peak amplitude of 0.5 km/s superimposed onto a constant velocity background of 2 km/s.

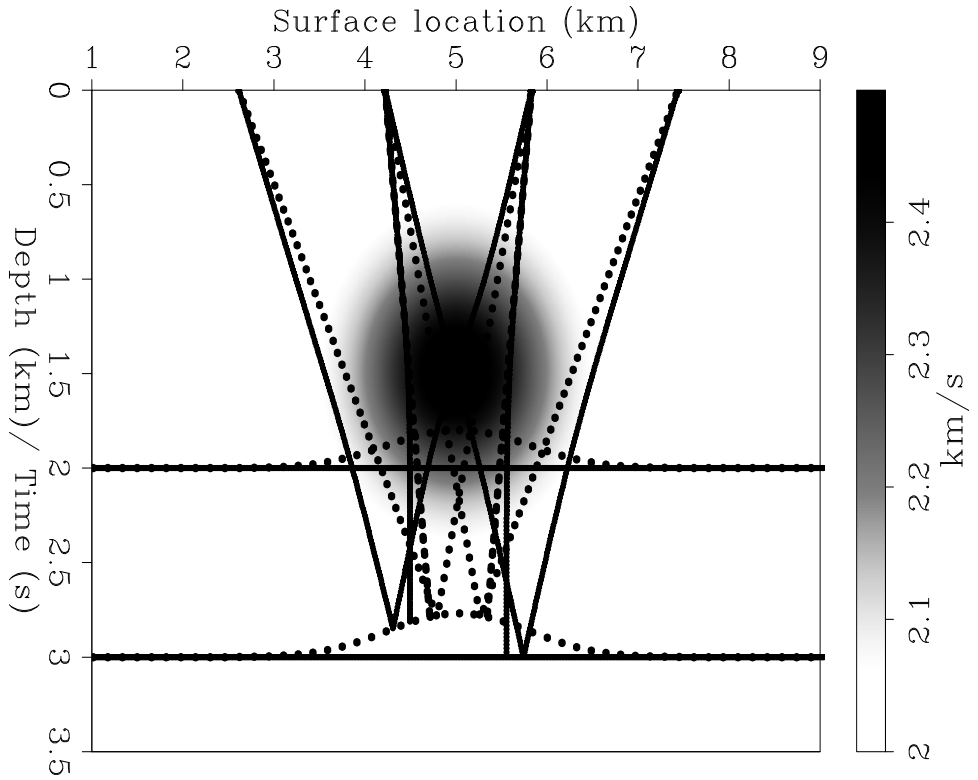


Figure 4: True velocity model with superimposed both the starting (dashed) and true reflectors (solid) in both the $(z,x)$ and $(\tau,\xi)$ domains. A few reflected raypaths are superimposed onto the model. foceiko-Comp-flat [NR]

We positioned two flat reflectors. The deep reflector at 3 km is below the anomaly, while the shallow one at 2 km cuts through the anomaly. Figure 4 shows the true velocity model with superimposed both the starting (dashed lines) and the true reflectors (solid lines) along with few reflected raypaths. The raypaths on the left are traced in the $(\tau,\xi)$ domain while the raypaths on the right are traced in the $(z,x)$ domain. We can notice how both the reflectors and the rays move less in the $(\tau,\xi)$ representation.

Figure 5 shows comparison of the linearization errors in modeling traveltimes of the reflections from the deeper reflector. The errors are shown as a function of the midpoint for two different offsets. The thicker lines show the errors at zero offset, and the thinner lines show the errors at 3.2 km offset. The solid lines show the error in the $(z,x)$ domain and the dashed lines show the errors in $(\tau,\xi)$ domain. There is no significant differences in errors between the two domains. This result is not surprising since the background model is constant and the deeper reflector does not interfere with the anomaly.

Figure 6 shows comparison of the linearization errors in modeling traveltimes of the reflections from the shallower reflector. In this case the reflector interferes with the anomaly, and the errors for $(\tau,\xi)$ domain tomography are smaller. We explain these differences with the interference between the reflector movements and the velocity perturbations.

The second example has a more complex background velocity. A fast body (e.g. salt layer) is placed at depth, below a shallow positive anomaly. The shallow anomaly distorts the time image of the fast body. Because we assume that the shallow anomaly is not known, the fast body is vertically distorted in the $(z,x)$ domain starting model. On the contrary, in the $(\tau,\xi)$ domain the fast body has the same position in both the starting and true model. Figure 7 show the true velocity model and the reflector geometry in the $(z,x)$ domain. A contour plot of the starting model is superimposed onto the true model to illustrate the vertical distortion of the fast body. A sample of zero-offset rays for both the true (solid lines) and the starting models (dashed lines) are superimposed onto the velocity model. Figure 8 shows the equivalent objects of Figure 7, but in the $(\tau,\xi)$ domain.

Figure 9 show the linearization errors for zero-offset reflections and 2 km offset reflections. The solid lines show the error in the $(z,x)$ domain and the dashed lines show the error in $(\tau,\xi)$ domain. The errors for $(\tau,\xi)$ domain tomography are smaller, although the differences are not that large.

The final example is similar to the previous one, except that the shallow anomaly is negative instead of positive. In this case, surprisingly, the linearization errors shown in Figure 10 are lower for the $(z,x)$ domain tomography. than for the $(\tau,\xi)$ domain tomography. A possible explanation of these results is that, by coincidence, the additional errors in the $(z,x)$ domain caused by the reflectors and velocity model movements have opposite sign of the errors caused by the non-linear behavior of the forward modeling.

A comparison of Figure 7 with Figure 8 shows that the deep, fast body shifts vertically in $(z,x)$ domain (Figure 7) while it is stationary in the $(\tau,\xi)$ (Figure 8). Because of the depth shift of the fast body, the velocity perturbations in the $(z,x)$ domain are a dipole with a positive and negative anomaly close to each other. Usually tomographic inversions strongly penalize features like a dipole that are rapidly variant in space. They are difficult to resolve by tomography, and they can lead to divergence if not kept in check. Therefore correcting the initial distortion by a linearized inversion would be difficult; a full migration followed by reflector interpretation are probably required.

## CONCLUSIONS

The focusing eikonal equation exactly models the traveltimes in a heterogeneous medium parametrized by the vertical traveltime $\tau$ in place of depth $z$. The solutions of the focusing eikonal can be efficiently computed by solving the associated ray tracing equations.

A potential application of the focusing eikonal that we intend to investigate further is reflection tomography. Our preliminary analysis of the linearization errors for $(z,x)$ domain tomography and $(\tau,\xi)$ domain tomography shows that, when reflectors' movements interfere with velocity perturbations, $(\tau,\xi)$ tomography behaves more linearly than $(z,x)$ tomography. However, we feel that our analysis is only preliminary. A natural next step is to analyze the back-projection operators, and compare their properties. Further on we should perform full non-linear tomographic tests.

## ACKNOWLEDGMENTS

The first time that the first author (BB) heard about "tracing rays in time" was from Francis Muir few years ago. He heard about $\tau$-rays again this summer while visiting Elf's Geophysical Research Center in London.

## REFERENCES

Alkhalifah, T., Fomel, S., and Biondi, B., 1997, Time-domain anisotropic processing in arbitrarily inhomogeneous media: SEP–**95**, 77–99.

Fomel, S., 1997, A variational formulation of the fast marching eikonal solver: SEP–**95**, 127–147.

Hatton, L., Larner, K. L., and Gibson, B. S., 1981, Migration of seismic data from inhomogeneous media: Geophysics, **46**, no. 5, 751–767.

Hubral, P., 1977, Time migration - some ray theoretical aspects: Geophys. Prosp., **25**, no. 4, 738–745.

Larner, K. L., Hatton, L., Gibson, B. S., and Hsu, I. C., 1981, Depth migration of imaged time sections: Geophysics, **46**, no. 5, 734–750.

Raynaud, B. A., and Thore, P., 1993, Real time migration operators simulated by anisotropic ray tracing: 55th Mtg. Eur. Assoc. Expl Geophys., Abstracts.

Sethian, J. A., and Popovici, A. M., 1997, Three-dimensional traveltime computation using the fast marching method: submitted to Geophysics.

Stork, C., and Clayton, R. W., 1991, Linear aspects of tomographic velocity analysis: Geophysics, **56**, no. 4, 483–495.

## APPENDIX A

## REFLECTIONS IN $(\tau,\xi)$

In this Appendix we derive the relationships between the ray parameters of the $\tau$-rays reflected from a planar dipping reflector, and the ray parameters of the incident rays. We start by the equivalent relationship for $z$-rays. The ray parameters of the reflected $z$-ray $\left(p_{x\Uparrow}, p_{x\Uparrow}\right)$ are related to the ray parameters of the incident $z$-rays $\left(p_{x\Downarrow}, p_{x\Downarrow}\right)$ as follows:

$$\begin{aligned} p_{x\Uparrow} &= p_{x\Downarrow}\cos 2\alpha_z + p_{z\Downarrow}\sin 2\alpha_z \\ p_{z\Uparrow} &= p_{x\Downarrow}\sin 2\alpha_z - p_{z\Downarrow}\cos 2\alpha_z \end{aligned} \tag{A-1}$$

where $\alpha_z$ is the dip angle of the reflector.

The ray parameters of the $\tau$-rays are related to the ray parameters of the $z$-rays by

$$\begin{aligned} p_x &= p_\xi + p_\tau \sigma_f \\ p_z &= p_\tau \frac{2}{V}. \end{aligned} \tag{A-2}$$

Substituting equation A-2 into equation A-1 we get

$$p_{\tau\Uparrow} = p_{\xi\Downarrow}\frac{V}{2}\sin 2\alpha_z + p_{\tau\Downarrow}\left(\frac{\sigma_f V}{2}\sin 2\alpha_z - \cos 2\alpha_z\right) \tag{A-3}$$

$$p_{\xi\Uparrow} = p_{\xi\Downarrow}\left(\cos 2\alpha_z - \frac{\sigma_f V}{2}\sin 2\alpha_z\right) + p_{\tau\Downarrow}\left[2\sigma_f \cos 2\alpha_z + \left(\frac{2}{V} - \frac{\sigma_f^2 V}{2}\right)\sin 2\alpha_z\right].$$

The dip $\alpha_z$ of a reflector in depth is related to the time-dip angle $\alpha_\tau$ by

$$\tan\alpha_z = \frac{V}{2}\left(\tan\alpha_\tau - \sigma_f\right). \tag{A-4}$$

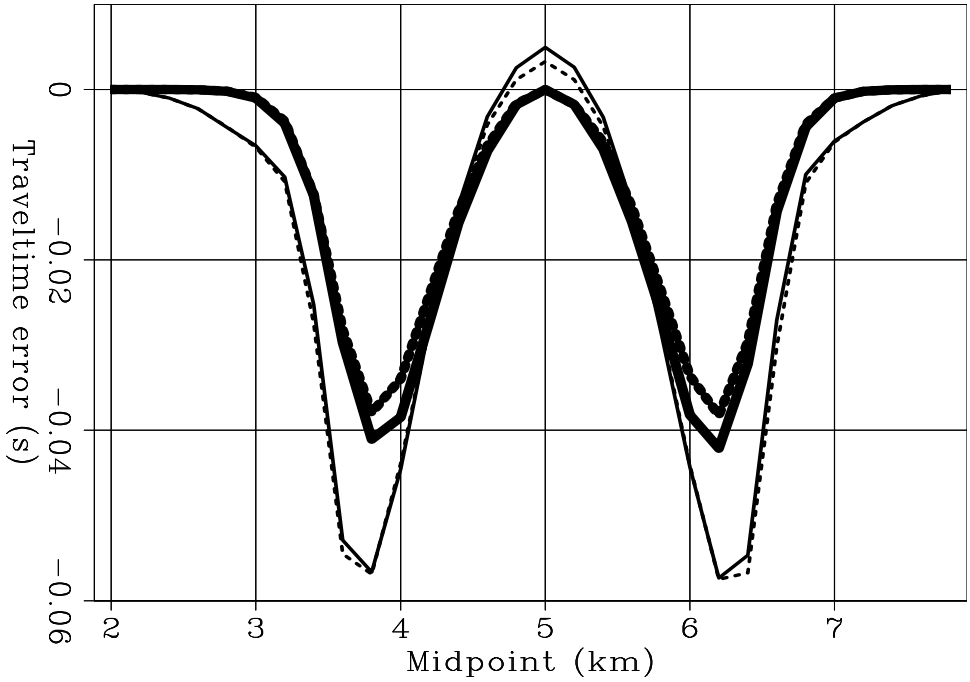


Figure 5: Linearization errors for the deep reflector at zero offset (thick) and 3.2 km offset (thin): solid lines for $(z,x)$ domain tomography and dashed lines for $(\tau,\xi)$ domain tomography. foceiko-Comp-tomo-flat [NR]

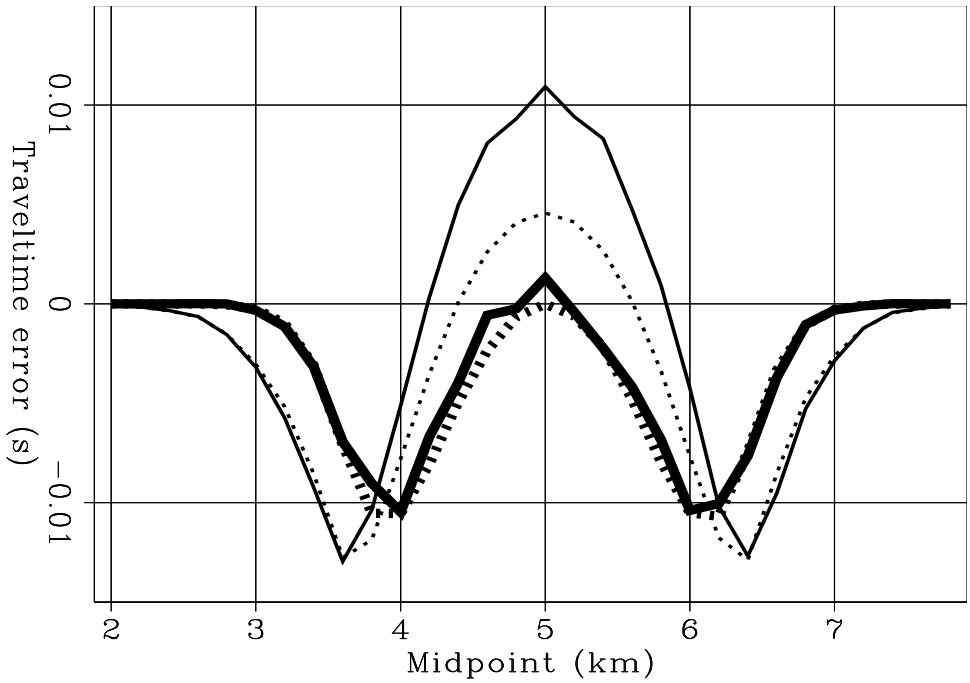


Figure 6: Linearization errors for the shallow reflector at zero offset (thick) and 3.2 km offset (thin): solid lines for $(z,x)$ domain tomography and dashed lines for $(\tau,\xi)$ domain tomography. foceiko-Comp-tomo-anom [NR]

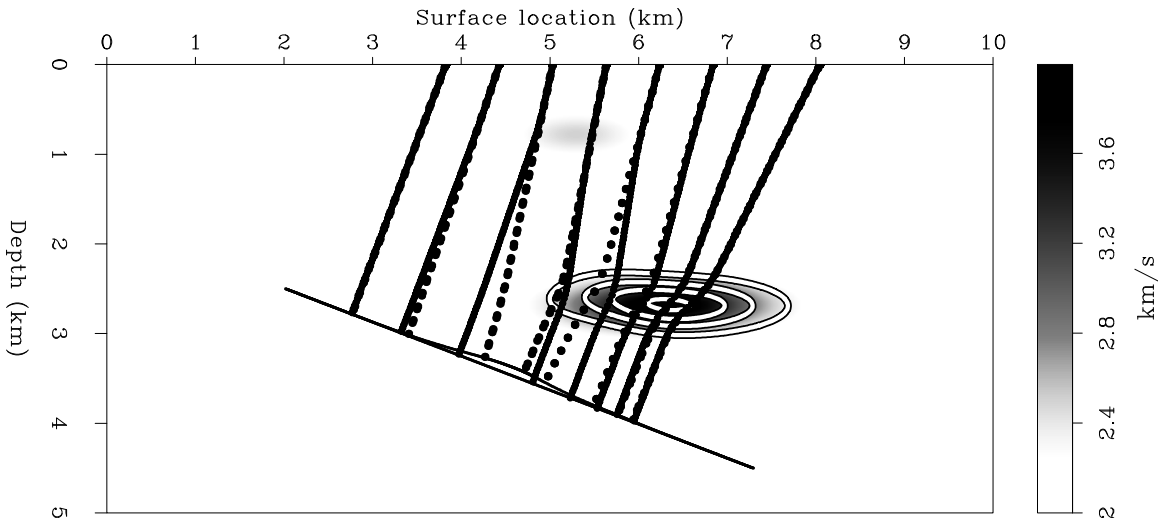


Figure 7: True velocity model in $(z,x)$ domain with a superimposed a contour plot of the starting velocity model. The reflector geometries and a few zero-offset raypaths are superimposed onto the model. foceiko-Movez-dip [NR]

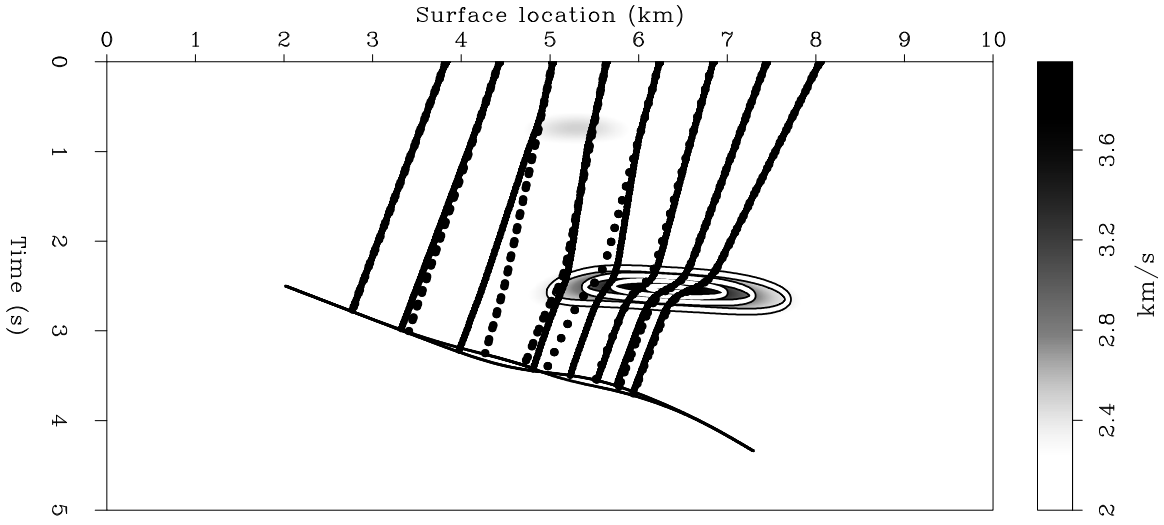


Figure 8: True velocity model in $(\tau,\xi)$ domain with a superimposed a contour plot of the starting velocity model. The reflector geometries and a few zero-offset raypaths are superimposed onto the model. foceiko-Movetau-dip [NR]

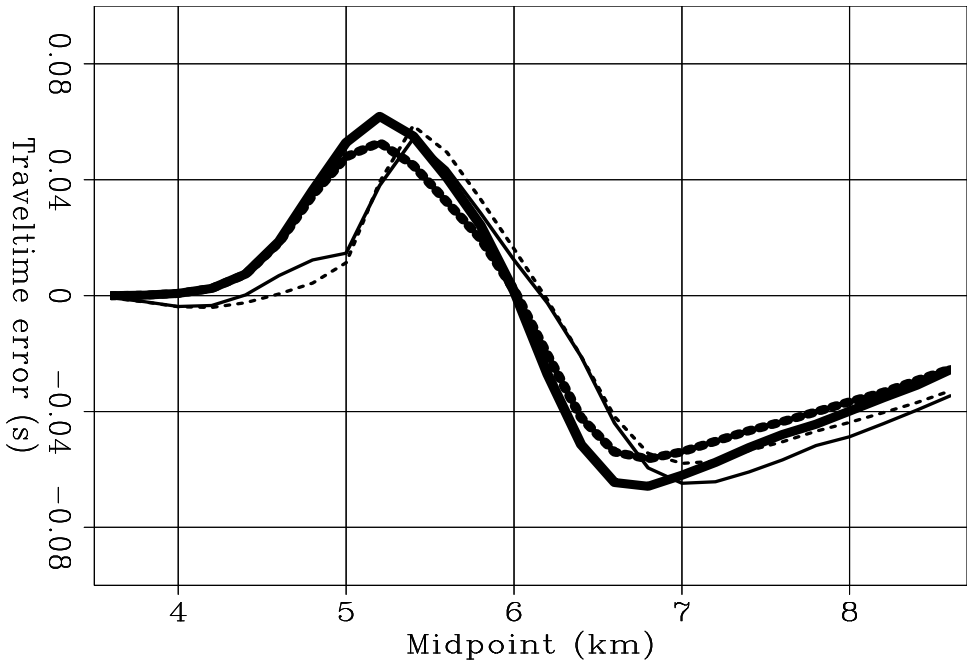


Figure 9: Linearization errors for the positive anomaly case at zero offset (thick) and 2 km offset (thin) (solid lines for $(z,x)$ domain tomography and dashed lines for $(\tau,\xi)$ domain tomography). foceiko-Comp-tomo-dip-pos [NR]

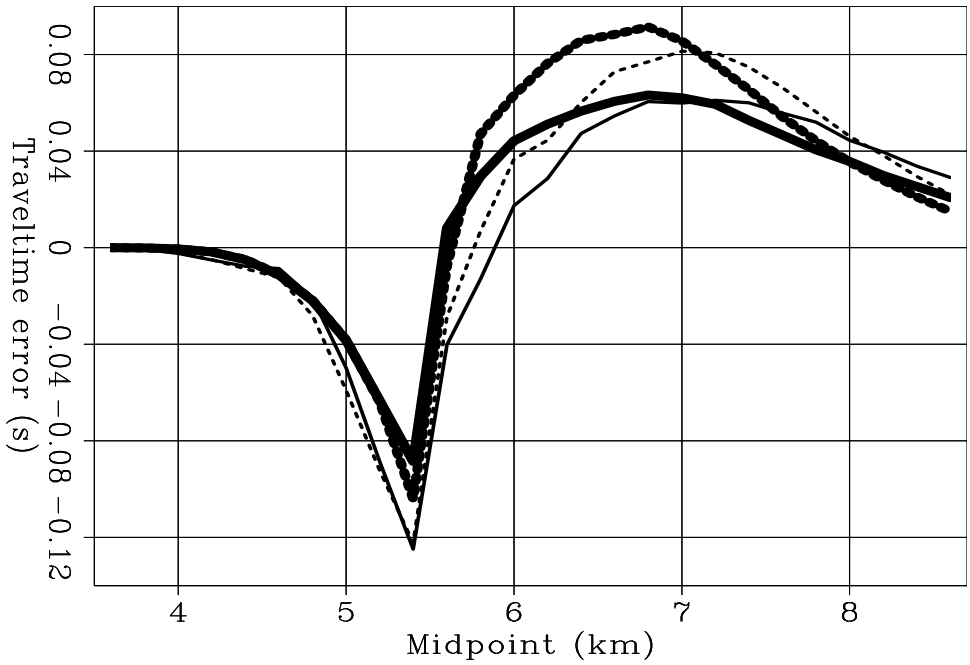


Figure 10: Linearization errors for the negative anomaly case at zero offset (thick) and 2 km offset (thin) (solid lines for $(z,x)$ domain tomography and dashed lines for $(\tau,\xi)$ domain tomography). foceiko-Comp-tomo-dip-neg [NR]